

# UC Irvine

## UC Irvine Previously Published Works

### Title

Complex fluorescence decay profiles: discrete models, stretched exponential, analytical models

### Permalink

<https://escholarship.org/uc/item/5q279175>

### Authors

Digman, M  
Gratton, E

### Publication Date

2012

### Copyright Information

This work is made available under the terms of a Creative Commons Attribution License, available at

<https://creativecommons.org/licenses/by/4.0/>

Peer reviewed

# 10

# The phasor approach to fluorescence lifetime imaging: Exploiting phasor linear properties

*Michelle A. Digman and Enrico Gratton*

## Contents

10.1 Introduction	235
10.2 The phasor “linear transformation”	236
10.3 The median filter applied to phasor component images	238
10.4 Maintaining the spatial resolution	239
10.5 Filtering in the phasor plot reveals hidden components	240
10.6 Linear combinations of molecular species in the same pixel: Quantitation of FRET	242
10.7 Exploiting the linear property to segment images	243
10.8 Cell phasor analysis	246
10.9 Conclusions	247
Acknowledgments	248
References	248

## 10.1 INTRODUCTION

The phasor approach to fluorescence lifetime imaging (FLIM) is emerging as a practical method for data visualization and analysis. The main feature of the phasor approach is that it is a “fit-free” analysis tool that provides quantitative results about mixtures of fluorophores, Förster resonant energy transfer (FRET), and autofluorescence [1–8]. Since phasor FLIM analysis is relatively simple, fast and accurate, its use is becoming more frequent [1,9]. A less emphasized feature of the phasor approach is that it provides a substantial new concept for FLIM analysis, which arises from the linear transformation of the fluorescence decay at each pixel. In this work, we explore consequences of using this linear transformation for improving the signal-to-noise ratio of FLIM data by applying filtering methods to the images of phasor components. It is well established that linear addition of phasors is crucial for facilitating data analysis and interpretation. It is less known that the linear phasor transformation opens up the possibility of decreasing the variance of FLIM images using simple data filtering. We also show that linear combination of phasors allows color coding of FLIM images on the basis of the fraction of molecular species without using fitting procedures. Finally, we show that image segmentation based on algorithms exploiting the intensity information present in the FLIM image is simplified since the result of the segmentation can be seen real time in the FLIM image.

The phasor approach to fluorescence lifetime analysis was first introduced by Jameson et al. [10] in the context of single-point lifetime measurements. Recently, the phasor idea was proposed for the analysis of multiexponential decaying systems from cuvette measurements [11,12]. In 2008, Digman et al. [5] used the phasor approach to analyze FLIM data. In the Digman et al. paper, three fundamental new ideas were introduced: (1) phasor fingerprinting for the identification of molecular species, (2) linear combination of molecular species (as opposed to linear combination of exponential components), and (3) FRET analysis in FLIM using trajectories in the phasor plot. More importantly, in the work of Digman et al., it was emphasized that each molecular species has a specific location in the phasor plot and that the identification of a species in a sample does not require the resolution of the decay into exponential components.

## 10.2 THE PHASOR "LINEAR TRANSFORMATION"

In the FLIM analysis method, a fluorescence decay curve is collected at every pixel of an image. The specific method of data collection can be both in the time and in the frequency domain [13]. Here we will assume that data are collected in the time domain under the form of the time-correlated single-photon counting (TCSPC) decay histogram at each pixel [14]. However, the derivations and discussions of this chapter apply to data collected in the frequency domain as well. Therefore, we start from the TCSPC collection of fluorescence decay curves at each pixel of an image. In the phasor approach, the decay  $I(t)$  at each pixel is transformed into two coordinates in a Cartesian plot according to the following equations:

$$s_i(\omega) = \int_0^{\infty} I(t) \sin(n\omega t) dt \Big/ \int_0^{\infty} I(t) dt, \quad g_i(\omega) = \int_0^{\infty} I(t) \cos(n\omega t) dt \Big/ \int_0^{\infty} I(t) dt \quad (10.1)$$

where,  $g_i(\omega)$  and  $s_i(\omega)$  are the  $x$  and  $y$  coordinates of the phasor in the phasor plot, respectively;  $\omega$  is the angular repetition frequency of the excitation source; and  $n$  is the harmonic frequency (typically 1 or 2).

In the frequency domain, the phases ( $\phi$ ) and the modulations ( $m$ ) of the signal are measured at several harmonic frequencies. In this case, the phasor coordinates are given by

$$s_i(\omega) = m \sin(\phi), \quad g_i(\omega) = m \cos(\phi) \quad (10.2)$$

In the phasor plot, the values of  $g_i(\omega)$  and  $s_i(\omega)$  are thought of as coordinates of vectors with origin in the (0,0) point. Phasors are normalized so that the coordinates have no units. In the phasor plot, the horizontal axis is used for the  $g$  (or cosine) transform. The values of  $g$  are between 0 and 1. The vertical axis is for  $s$  (the sine transform), which has a value between 0 and 0.5. These phasors follow the normal vector algebra. Their coordinates can be added or subtracted.

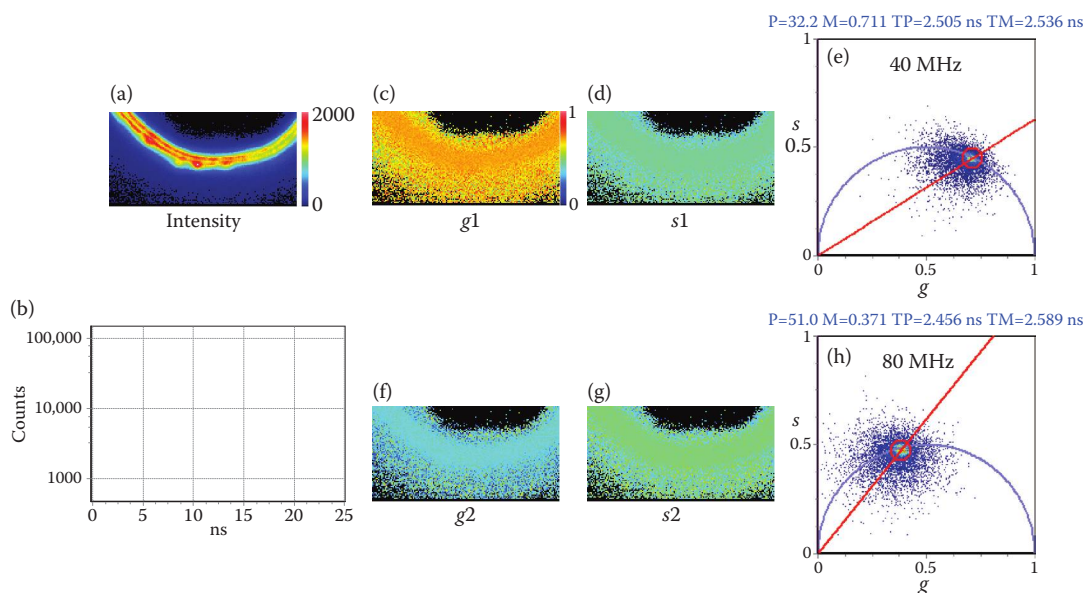


**Figure 10.1** (a) Intensity image. The fluorescence is from a protein construct containing GFP. (b) Average decay (all pixels). The laser repetition frequency is 40 MHz. (c)  $g_1$  image. The color code (from 0 to 1) is shown in the side bar of this panel. (d)  $s_1$  image, same color scale as in (c). (e) Phasor histogram of the first harmonics at 40 MHz corresponding to images  $g_1$  and  $s_1$ . (f)  $g_2$  image at 80 MHz, same color scale as for (c). (g)  $s_2$  image at 80 MHz, same color scale as for (c). (h) Phasor histogram of the second harmonics at 80 MHz. Data shown in this figure were collected with a Picoquant HARP300 system in the laboratory of Professor Claus Siedel, Dusseldorf, Germany. Excitation was from a picosecond laser at 488 nm, and emission was measured using a hybrid photomultiplier detector and a band-pass filter in the region 510–530 nm.

After the phasor transformation, for each pixel, we store five numbers, which are the total intensity,  $g_1$ ,  $g_2$ ,  $s_1$ , and  $s_2$ . The  $g$  and  $s$  are the coordinates of the phasor transform at two harmonics of the laser repetition frequency, respectively, for each pixel of the image. The total intensity at each pixel must be stored separately so that the sum implicit in the terms of Equation 10.1 can be used to combine the decay from adjacent pixels such as in binning. These five sets of numbers provide five matrices (images), which are combined to provide the phasor histogram at each harmonic, as shown in Figure 10.1. As the phasor approach is gaining popularity, images at more than two harmonics are stored, which enables better separation of molecular species when their locations in the phasor plot are very close to each other (Figure 10.1e and h).

The decay at each pixel (Figure 10.1b) is transformed using Equation 10.1 in matrices of pixels (images) corresponding to the coordinates of the phasors (Figure 10.1c and d). The phasors are then plotted in the phasor histogram, as shown in Figure 10.1e. A phasor transformation is also performed for the second harmonics of the laser repetition frequency (Figure 10.1f and g), and a second phasor plot is generated at the second selected harmonic (Figure 10.1h). In principle, we could have as many harmonics as the data

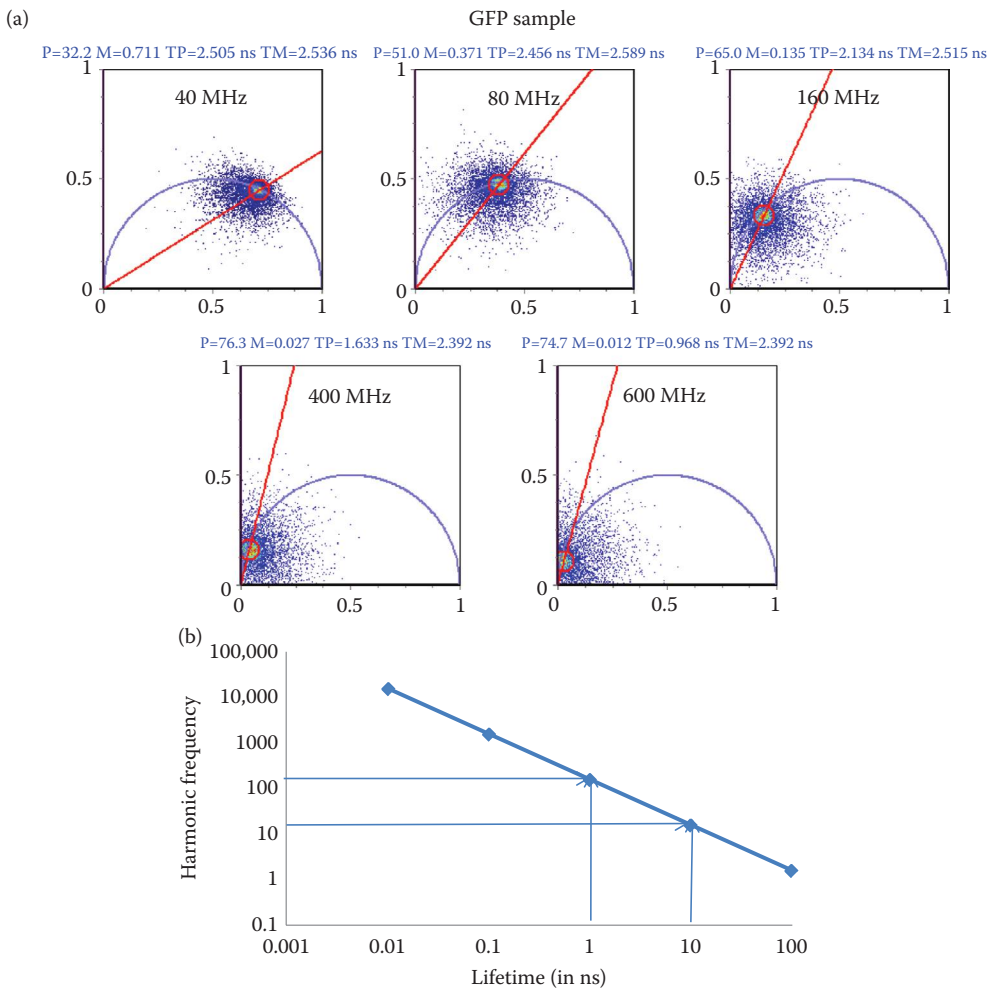


**Figure 10.2** (a) For the GFP sample shown in Figure 19.1, the phasor histogram is shown for five selected harmonics from 40 MHz (fundamental) to 600 (MHz), the 15th harmonics. (b) Plot of the frequency that provides the best resolution as a function of the lifetime of the probe. For lifetime values in the range of 1–10 ns, the best frequency is in the range of 16–160 MHz.

support, that is, equal to half the number of bins used to collect the data in the TCSPC technique. In the following example, we show calculations of five harmonics up to 600 MHz. The phasor histogram does not broaden very much as the frequency is increased for the example above. As the frequency increases (from 40 to 600 MHz), the phasor histogram shifts along the universal circle toward the (0,0) coordinate. The best frequency at which we will have the maximal sensitivity to changes in the phasor location is when the phasor is located in the central region of the phasor plot (Figure 10.2, between 40 and 80 MHz) [15]. For example, for a probe with a lifetime of 2.5 ns (GFP) the best modulation frequency is about 60 MHz (Figure 10.2b).

Generally, a laser repetition rate in the range of 20–40 MHz is ideal for FLIM analysis of biological samples. Note that the optimal condition for FLIM data collection for typical biological sample is realized if both the laser pulse and the detector response are in the subnanosecond range. On the contrary, if the repetition rate is too high, the phasors of various molecular species will be crowded in a small area of the phasor plot, and their separation becomes problematic.

### 10.3 THE MEDIAN FILTER APPLIED TO PHASOR COMPONENT IMAGES

The phasor transformation provides “images” of the decay for the  $g$  and  $s$  components. These images can be refined using various image processing tools, providing an entirely new approach to FLIM data analysis. Note that this image refinement approach is not available in the common time-domain data analysis based on fit methods of data reduction.

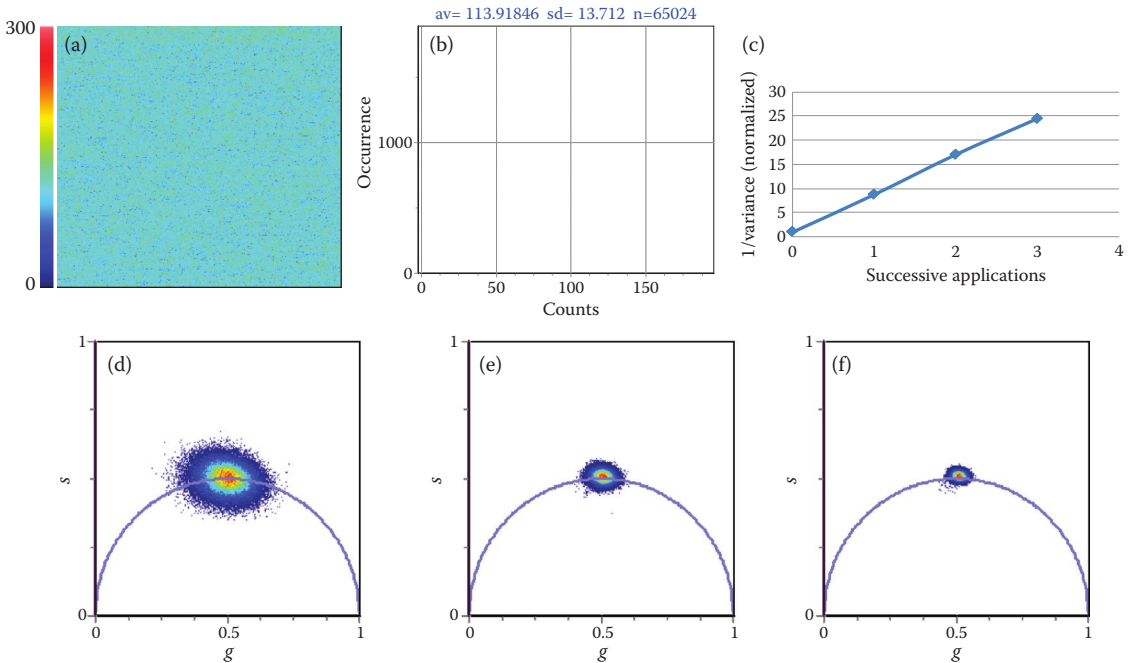
In FLIM data collection, the calculation of the lifetime at one pixel has generally a relatively large error due to the limited number of photons that are collected at any one pixel [13]. For example, if at one pixel, 100 photons are collected, error propagation shows that the uncertainty in the measured lifetime, assuming that the decay is exponential, is about 20% of the value of the lifetime [13]. Since the variance (square of the error) decreases linearly with the number of photons collected, it is a common procedure in FLIM to average neighboring pixels, for example, in a  $3 \times 3$  pixel region. This is done by summing the decay histograms in nine adjacent pixels and then assigning this average histogram to the center of this  $3 \times 3$  pixel region. The binning procedure decreases the spatial resolution of the image, which is a problem.

Figure 10.3 shows an experiment of FLIM data collection for a solution of rhodamine 110. The average pixel count is 114, and the image has  $256 \times 256$  pixels (Figure 10.3b). The average lifetime of rhodamine 110 is 4.0 ns, and the standard deviation of the average pixel lifetime determination is 0.648 ns (16% error). By binning pixels three by three, the standard deviation decreases to 0.216 ns (5.4% error). However, this operation cannot be repeated since the spatial resolution is also strongly degraded. The binning procedure gives pixilated images, and it becomes difficult to distinguish specific cellular features to be associated with lifetime values.

We describe here a procedure used in the phasor approach that maintains the resolution of the original image while dramatically improving the determination of the phasor in one pixel. In the phasor approach, we can follow a totally different procedure to reduce the noise of the phasor location. Since the coordinates of the phasor are additive, we treat the coordinates  $g_i$  and  $s_i$  as two images. Filtering procedures are then applied to these two images, resulting in a dramatic reduction of the variance of the position of the phasors (Figure 10.3d through f). Generally, we use a  $3 \times 3$  convolution filter based on the median operation. The median filter does not reduce the resolution, but it tends to sharpen the borders, as will be shown later. The filter can be applied successively to decrease the uncertainty of the phasor location. The inverse of the variance of the phasor determination changes linearly with the number of filter applications (Figure 10.3c).

In Figure 10.4, we describe the operation of the median filter since this is a relatively unknown method to this field. We show in Figure 10.4 the principle of the general operation of a convolution filter. For a discussion of filters applied to images, see the tutorial at <http://micro.magnet.fsu.edu/primer/java/digitalimaging/processing/medianfilter/index.html>.

For the purpose of illustration, we describe a convolution with a  $3 \times 3$  matrix, but other sizes of matrices can be used as well, such as  $5 \times 5$  or larger matrices. The median filter assigns the median value of the nine pixels to the central pixel of the  $3 \times 3$  region (Figure 10.4). The nine values are sorted in order of increasing value, and the central value is selected.



**Figure 10.3** Successive applications of the median filter to the  $g$  and  $s$  images reduce the variance of the phasor location. (a) Image of a slide of a solution of rhodamine 110. (b) Histogram of pixel counts. The average is about 114 counts. (c) The inverse of the variance changes linearly with the number of filter applications. (d) Original phasor distribution. (e) One application of the median filter. (f) Three applications of the median filter. In the phasor plot, some points appear outside the main distribution after filtering. These phasors are at the image border that is not filtered in the convolution procedure.

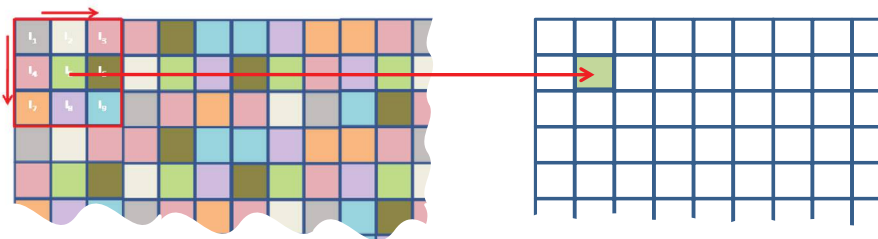


**Figure 10.4** Operation of the convolution filter. An image is analyzed using a moving window of  $3 \times 3$  pixels. In the resulting image on the right, a pixel corresponding in location to the central pixel of the  $3 \times 3$  moving window is assigned with a value according to a logical or arithmetic operation. In the median filter, the pixel value is the median of the values of the nine pixels in the convolution window (red box). In the conventional smoothing filter, the pixel value is the arithmetic weighted mean of weights assigned to each value of the exploring matrix. By moving the window one pixel at a time both in the  $x$  and  $y$  direction, we obtain a filtered image. The border of the image is not filtered.

## 10.4 MAINTAINING THE SPATIAL RESOLUTION

Figure 10.5a schematically shows the operation of the median filter and comparison with the common smoothing filter. The specific weights used for the smoothing filter in this example are shown in Figure 10.5a. The image in Figure 10.5b (fluorescence from a tissue sample) shows bright fluorescent granules as well as broad structures that correspond to cells. After three applications of the median filter, the image

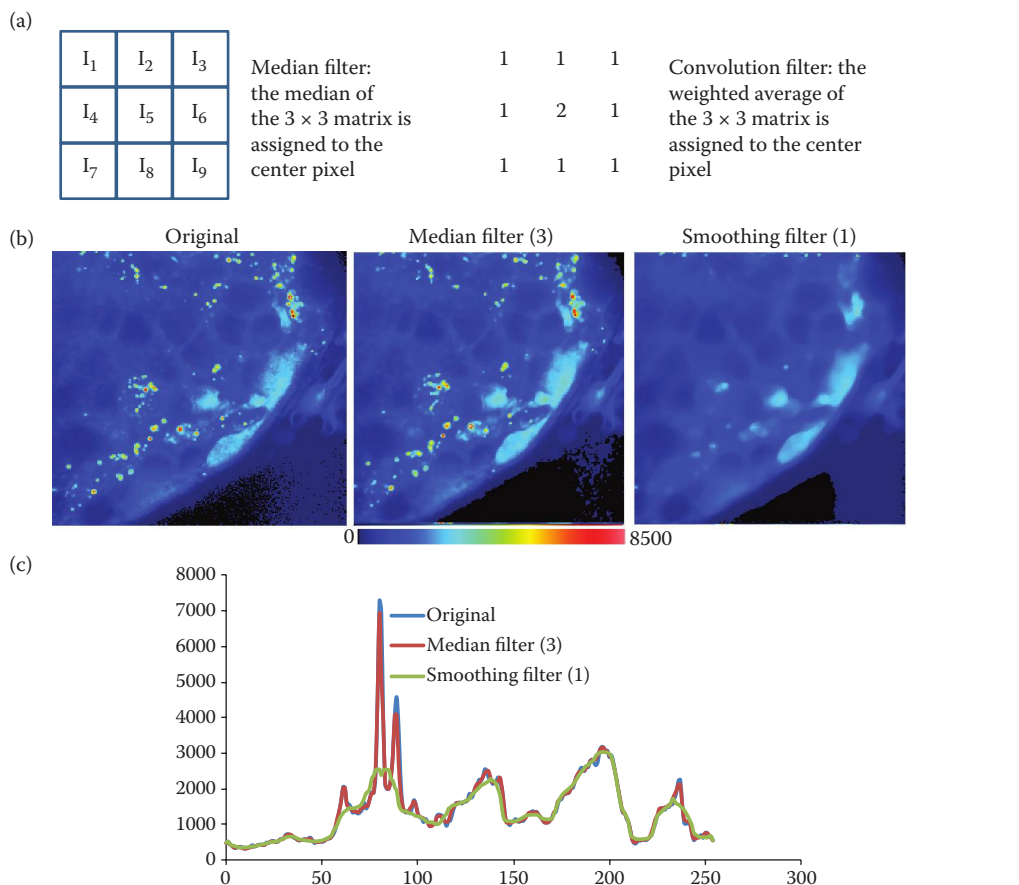


**Figure 10.5** (a) Schematic representation of the  $3 \times 3$  median and smoothing filters. A  $3 \times 3$  region of the image is systematically explored. The value of the center pixels of the  $3 \times 3$  pixel region is substituted with the median value (median filter) or with the weighted average of the intensity values of the  $3 \times 3$  region each multiplied by the corresponding weighted matrix value (smoothing filter). (b) Comparison of the original image, the image after three applications of the median filter, and after one application of the smoothing filter. (c) Profile of the horizontal line 128 of the image in (b).

resolution is not affected, and the granules are still visible. Figure 10.5c shows the profile of the horizontal line 128 of the image. The original image and the image processed with the median filter have the same resolution, and the bright spots are maintained. Instead, after application of the weighted moving average filter, the image resolution is greatly degraded. The bright spots have disappeared, and only the broad features are maintained (Figure 10.5c).

## 10.5 FILTERING IN THE PHASOR PLOT REVEALS HIDDEN COMPONENTS

Successive application of the median filter to the  $g$  and  $s$  images sharpens the phasor plot. Features that were invisible in the raw phasor plot could become distinct after this filtering procedure. Figure 10.6 shows a FLIM measurement of a cell in which the membrane is labeled with a protein construct that contains the GFP protein (same sample as in Figure 10.1). The count histogram of the original image shows that there is a bright region of the image (the cell wall) with about 1200–1400 counts per pixel (Figure 10.6b). The average lifetime image histogram shows a complex distribution, with a relatively narrow lifetime distribution component arising from the bright regions of the image and a broad pedestal arising from the



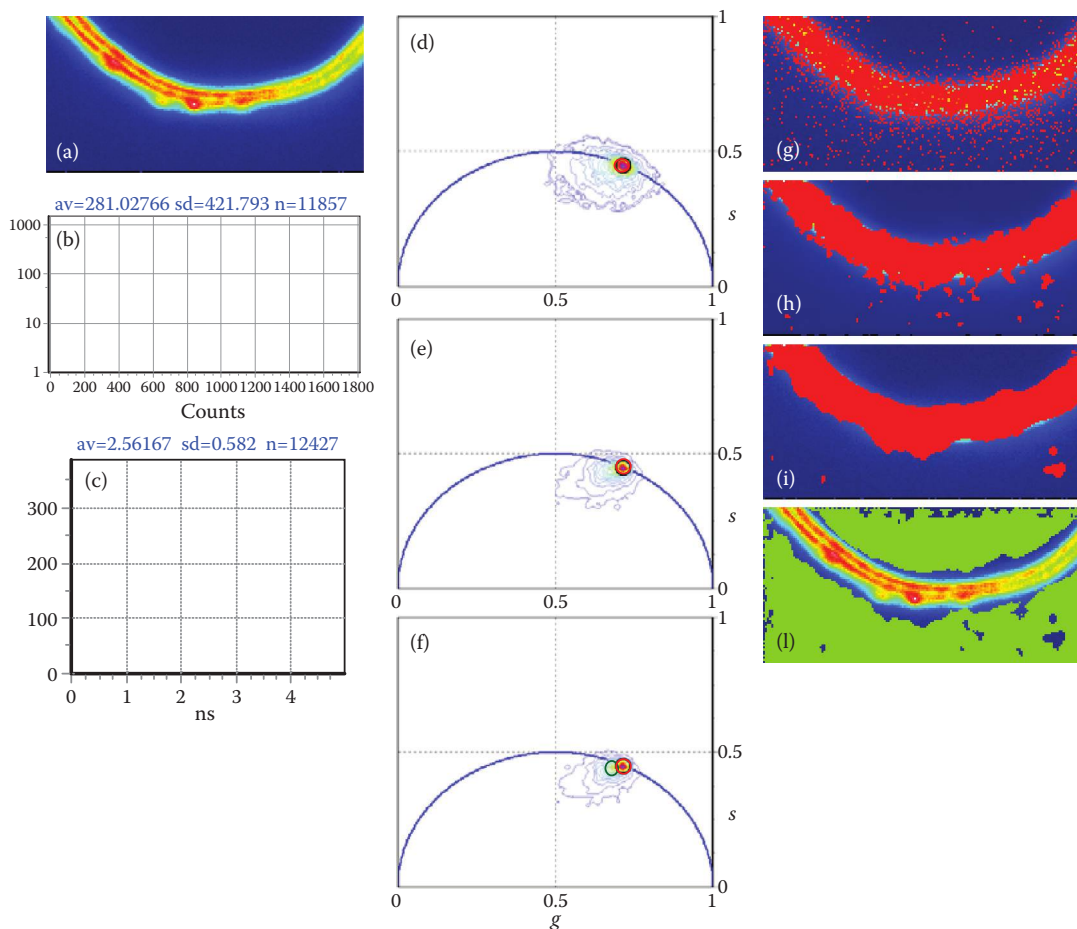


**Figure 10.6** Successive applications of the median filter reveal the origin of hidden components. (a) Image of GFP construct in a cell wall. (b) The histogram of counts shows that at the cell wall, there are about 1200–1400 counts. (c) Average lifetime distribution. (d) Raw phasor distribution. (e) Phasor distribution after one application of the median filter. (f) Phasor distribution after three applications of the median filter. (g) Selecting pixels within the red cursor in the phasor plot (d); mainly selects pixel of the cell wall but also other pixels. (h) After one application of the median filter (e), the phasor distributions becomes sharper, and most of the pixels of the cell wall are selected by the small red cursor. (i) After three applications of the median filter (f), the distribution becomes even sharper. A second minor contribution is now appearing as shown in Figure 10.3f by the green circle. (j) The phasor in this region corresponds to pixels in the region of the cell away from the membrane yet populated by the GFP construct. The lifetime in this region is slightly modified by the linear combination with a background, which, in this case, has a phasor at (0,0).

dim parts of the image (Figure 10.6c). The lifetime appears to be uniform everywhere, and the different counts statistics determine the broadening of the average lifetime distribution.

The phasor histogram shows a phasor distribution centered around 2.56 ns; the phasor histogram is not symmetric but elongated toward the origin of the phasor plot (Figure 10.6d). Successive applications of the median filter show that the phasor distribution is made of two components, which can be identified with the bright and dim parts of the image, respectively (Figure 10.6f, i, and j). In the dim parts, the phasor distribution is shifted toward the (0,0) point. This indicates that the “component” that is added to the GFP phasor is unmodulated background. This component can be easily separated, its location can be identified, and its relative contribution can be quantified at each pixel.

Also, the successive application of the median filter “packs” the phasor distribution without affecting the resolution of the image, as previously shown in Figure 10.5 for the tissue sample.



## 10.6 LINEAR COMBINATIONS OF MOLECULAR SPECIES IN THE SAME PIXEL: QUANTITATION OF FRET

Perhaps the most emphasized property of the phasor analysis is the linear combination of molecular species. Here, we show the graphical selection of pixels that are a linear combination of two phasors. The linear combination of the phasors corresponding to the two species can be used to map their distribution in an image using the phasor plot. In this example, we use the GTPase Rac1 biosensor construct from the Hahn lab [16,17]. The Rac1 is a dual-chain biosensor that consists of the CyPet-Rac1 protein and its binding domain, YPet-PBD. Upon activation with epidermal growth factor (EGF), the two proteins come together, and FRET between the CyPet and YPet fluorescent proteins can occur. COS7 cells were transfected with both donor (CyPet-Rac1) and acceptor (YPet-PBD) measured before and after EGF stimulation (donor channel). In the inactive state, the biosensor displays no FRET (the low FRET [L-FRET] state), while in the activated state, the biosensor shows high FRET (H-FRET) (Figure 10.7). In this experiment, a FLIM image (image 1 in Figure 10.7a) is measured before stimulation of the cell with epithelial growth factor (EGF). Then the cell is stimulated at frame 2, and subsequent frames were acquired every 10 s (frames 3–12). The phasor histogram in Figure 10.7b is the compound histogram from FLIM images 1–12. The fraction of FRET depends on the fractional intensity of the molecules that are in the active state. Experimentally, phasors distribute along a line joining the L-FRET and the H-FRET states (Figure 10.7b).

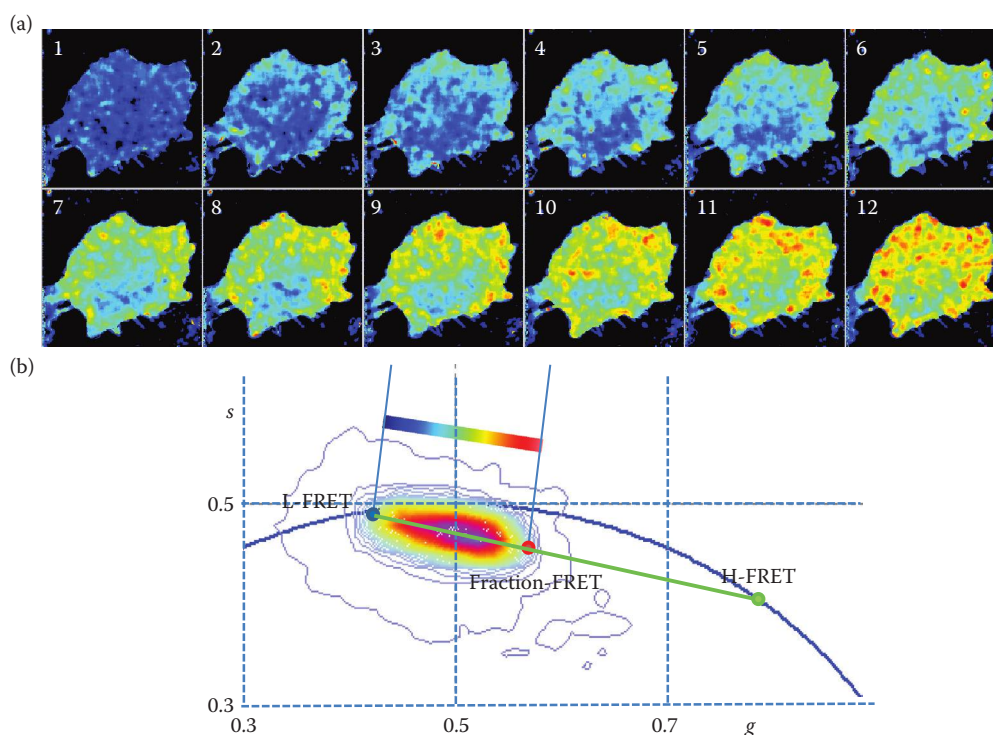


**Figure 10.7** (a) Sequence of FLIM images colored according to the scale of fraction of molecules in the L-FRET and H-FRET state obtained in (b). Image 1 is collected before activation with EGF. From 2 to 12, images were recorded every 10 s. (b) Compound phasor histogram of all images 1–12 of (a). The phasor histogram is elongated from L-FRET to H-FRET. Extrapolation of the points intercepting the universal circle of the best line through the histogram gives the L-FRET (blue point) and H-FRET (green point) state of the Rac1 biosensor. The maximal fraction H-FRET in a pixel (red point) is about 45%. The FLIM image is color coded according to the scale from L-FRET to the maximal fraction of FRET.

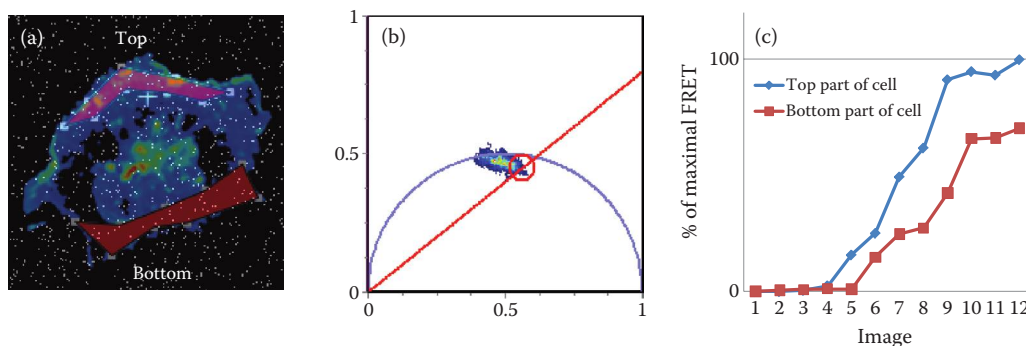


**Figure 10.8** (a) Cell measured in Figure 19.7, analyzed for pixels reaching maximal FRET in the top and bottom part of the cell. (b) Pixels in the red circle are considered as pixels with maximal FRET. (c) Fraction of pixels reaching maximal FRET in the FLIM image sequence of Figure 10.7.

Note that the experimental phasor distribution is along a line rather than along the universal circle. This implies that each pixel in the image contains a combination of L-FRET and H-FRET molecules. For this biosensor, there is no gradual change in FRET efficiency that would have given phasors on the universal circle. Instead, the intercept of the green line in Figure 10.7b with the universal circle gives the value of the H-FRET state (extrapolated lifetime of 1.10 ns), which, in this case, corresponds to a FRET efficiency of 54% (L-FRET state lifetime is 2.40 ns). The maximum fraction measured is about 45% (red point at fraction of FRET in Figure 10.7b).

Since the phasor distribution is along the line of linear combination of the L-FRET and H-FRET states, we color coded pixels in the image according to the color scale shown in Figure 10.7b for the FRET fraction range measured in this experiment. Note that there are no assumptions about the two FRET states or their locations. All points (red, blue, and green in Figure 10.7b) are directly derived from the phasor plot using graphical constructions. We can unequivocally derive the value of the maximal FRET efficiency of the biosensor and the fractional intensity contribution of H-FRET molecules in each pixel. To obtain the fraction of molecules (concentration), we must account for the relative quantum yield of the two states, which we assume are proportional to their lifetimes (the extrapolated points on the universal circle for this example). The formula for converting fractional intensities in concentration ratios is given in the work of Celli et al. [18].

In the example of the Rac biosensor, the FLIM images also provide the distribution of the active biosensor as a function of time. If we spatially section the image according to the regions outlined in Figure 10.8a in red, we can count the number of pixels that are in the active state by plotting their corresponding phasor distribution and selecting the maximal H-FRET state (red circle in Figure 10.8b) for the image sequence (1–12) in Figure 10.7a.

Pixels with maximal activation of the Rac biosensor start at frame 4–5 after stimulation with EGF and reach saturation at about frame 9–10. Note that in the bottom part of the cell, there are fewer pixels with maximal activation.

## 10.7 EXPLOITING THE LINEAR PROPERTY TO SEGMENT IMAGES

The linear property of the phasor representations is crucial for the separation and assignment of phasors to molecular species. In the following example, we show how to recognize features in the FLIM image characterized by different phasor clusters. Figure 10.9 shows a portion of tissue from a seminiferous mouse tube where stem cells express the Oct4-eGFP genetic fluorescent marker. In the intensity image (Figure 10.9a), we distinguish some broad features that could be identified with cells, a background where it is difficult to recognize any specific feature, and bright puncti covering various parts of the image. In

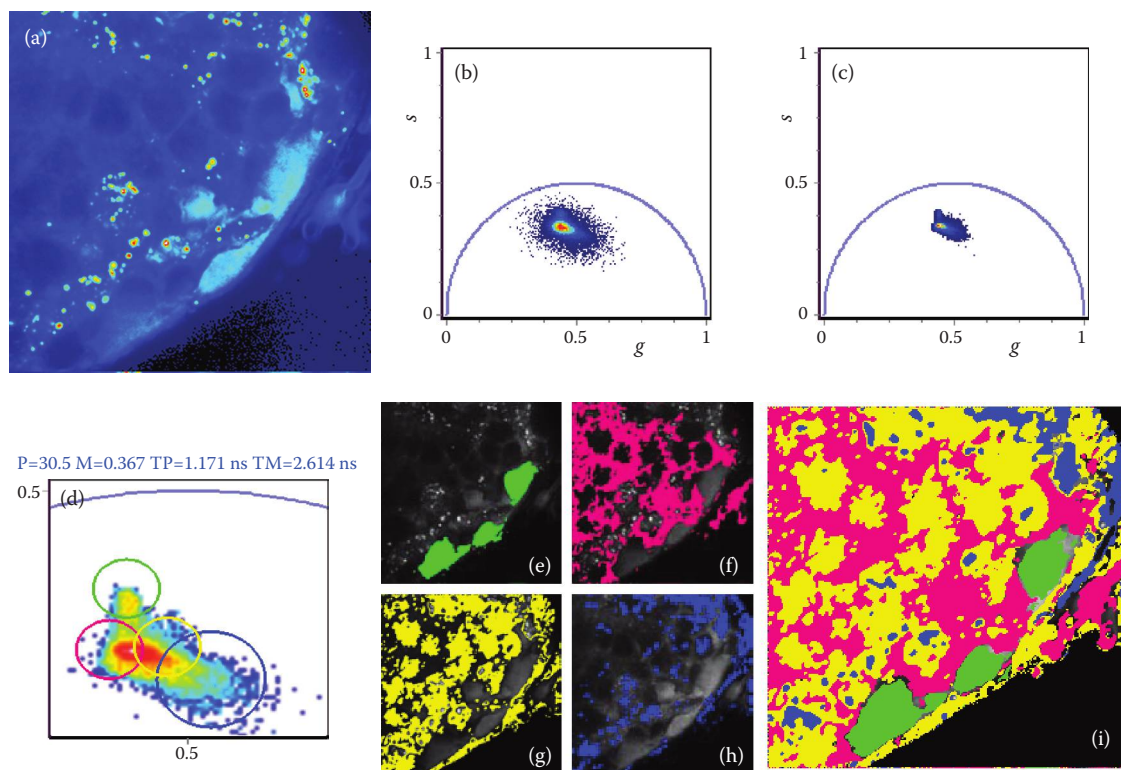


**Figure 10.9** (a) Image of an excised seminiferous tube tissue of a mouse with stem cells expressing the GFP-Oct4 gene using 900 nm excitation in the two-photon microscope. (b) Phasor histogram, showing a broad distribution. (c) After application of the median filter, the phasor histogram reveals clusters that can be identified with specific features in the tissue. (d) Zoomed-in region of the phasor plot in which four regions are selected. (e–h) The color-coded region selected in (d). (i) Compound image of the color-coded regions according to the selection in part (d).

Figure 10.9b we show the phasor plot of this image at 80 MHz obtained with a two-photon excitation at 900 nm. As previously noted, the cluster of phasors is rather broad, and it is impossible to assign specific phasors to each feature in the image. At this level of representation of the cluster of phasors, we need to unscramble the cluster to determine the contributions of the various molecular species to the overall compound phasor distribution. In Figure 10.9c, after the application of the median filter, we can distinguish several features in the phasor plot that we would like to identify with features in the image. In Figure 10.9d, we zoom in the phasor plot, and we select four different regions indicated by the four colored circles. The regions of the image selected on the basis of the clusters in the phasor plot are shown in Figure 10.9e through h, using the same color code in Figure 10.9d. Now we can clearly distinguish the stem cells that express the GFP in the Oct4 complex (Figure 10.9e), at least two cellular or extracellular compartments colored in yellow and pink, and another component at shorter lifetime in blue that could arise from blood vessels. The color-coded image in Figure 10.9i is the superposition of Figure 10.9e through h where the precedence of color (in case the selected regions superimpose) is from green to pink to yellow to blue, with the blue having the lower precedence.

If we try identifying the cellular features colored in pink and in yellow, the intensity image shows that the pink-colored pixels are located at the cell borders in the tissues, while the yellow pixels are located in the cell interior. For this experiment, we collected FLIM images using two excitation wavelengths in the two-photon microscope, at 790 and 900 nm, respectively. Figure 10.10 shows four different regions of the seminiferous tube of the same mouse. In Figure 10.10a through d, the excitation wavelength is 900 nm,

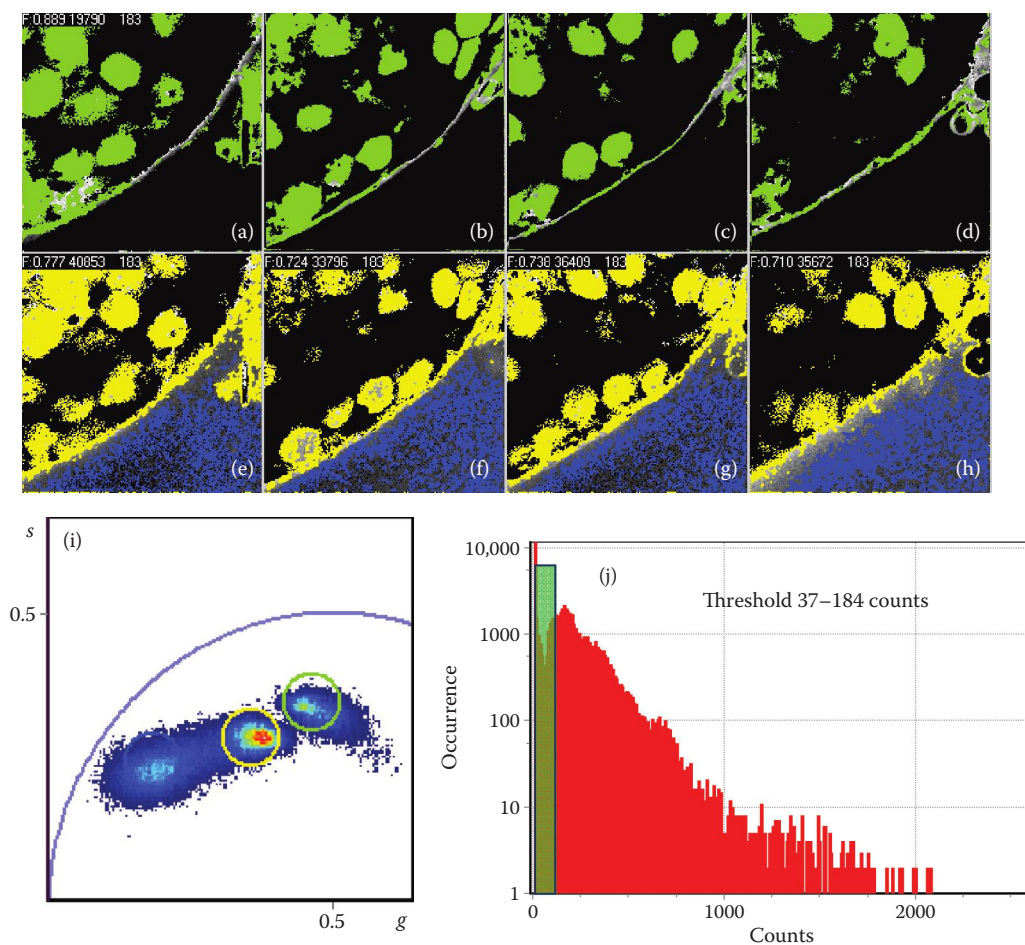


**Figure 10.10** Four different regions of the seminiferous tube of the same mouse tissue shown in Figure 10.9. (a–d) Excitation at 900 nm, (e–h) Excitation at 790 nm. (i) Compound phasor plot of the eight images (at both wavelengths) with the applied threshold. (j) Only pixels within a given value of intensity (low intensity) are selected, shown in the green rectangle.

and in Figure 10.10e through f, the excitation is at 790 nm. The compound phasor plot of the images is shown in Figure 10.10i. To better select the dim parts of the tissues corresponding to cells, we apply a threshold based on the intensity, as shown in the green bar in Figure 10.10j. The median filter was applied to these images. Clearly, both excitation wavelengths excite the same cells, but the emission must be from different molecular species since the phasor position is quite different when we select the same cells. Note that the stem cells and the bright spots have been excluded for the analysis of this image since they are bright.

In order to select the bright regions, we must plot the phasors corresponding to a higher threshold. In Figure 10.11 we select only the part of the image with high intensity. Images in Figure 10.11a through d are obtained exciting at 900 nm, and images in Figure 10.10e through h are excited at 790 nm. Figure 10.11i shows the compound phasor plot. This time, the cluster selected by the yellow circle in Figure 10.10i shows that the bright spots have the same phasor location at the two excitation wavelengths. By applying a threshold in regions of low and high intensity, we can identify and map different molecular species in great detail. The linear property of the phasors allows us to separate and navigate the phasor plot at ease.



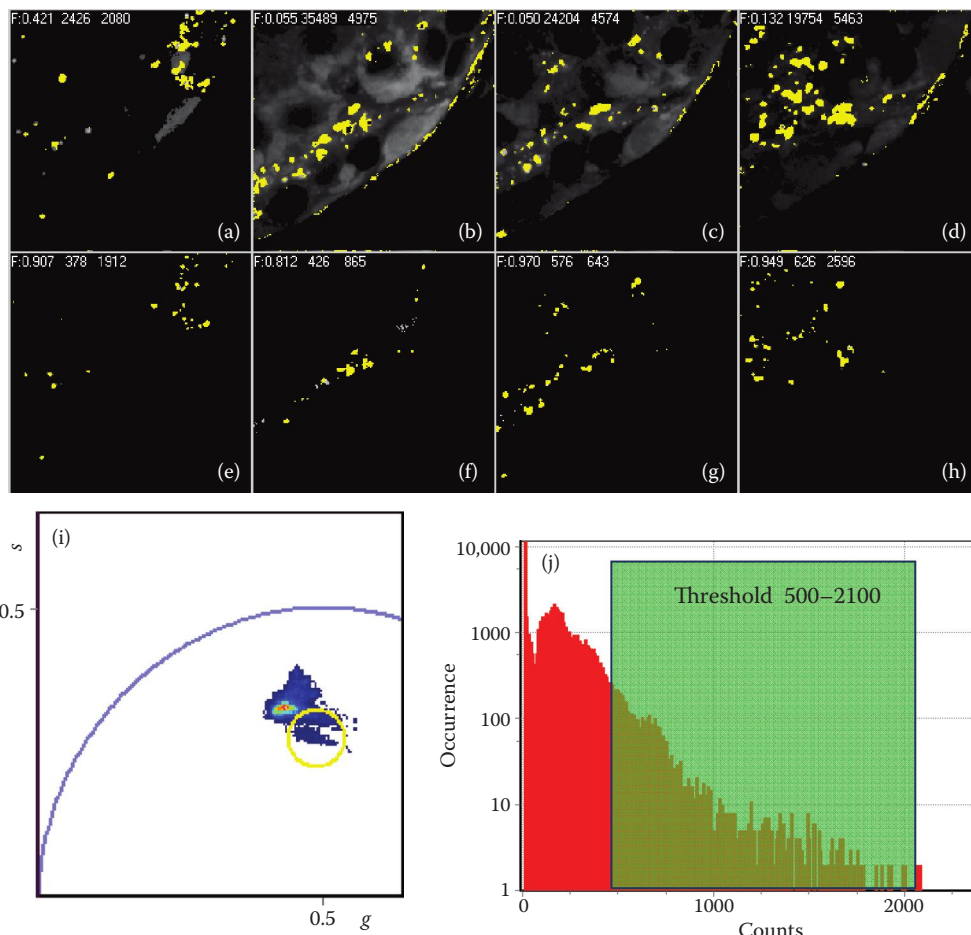


**Figure 10.11** Four different regions of the seminiferous tube of the same mouse. (a–d) Excitation at 900 nm. (e–h) Excitation at 790 nm. (i) Compound phasor plot of the eight images. (j) Only pixels within a given value of intensity (high intensity) are selected.

## 10.8 CELL PHASOR ANALYSIS

The cell phasor analysis is another segmentation approach that maps phasor contribution of individual cells and shows how neighboring cells in a tissue have diverse metabolic states [19]. In [Figure 10.12](#), we show the cell phasor segmentation analysis of the seminiferous tube. In this example, we segmented the image manually by tracing the contour of a cell by thresholding the intensity as to select only the fluorescent cells. We then calculate the average phasor of the selected region yielding one point on the phasor plot (noted by a star in [Figure 10.11c](#)). We can see that each cell has a slightly different position in the phasor plot. We note that the error of each cell phasor is very small since each region contains thousands of phasors. The position between cells becomes significant. Three of the cells (cells 2, 4, and 6) form a cluster in the direction of the GFP phasor. These cells will be identified as stem cells expressing the GFP-Oct4 genes, the true stem cells. The remaining cells (cells 1, 3, and 5) are bright, emitting in the green, but have a lifetime that is incompatible with the expression of GFP. On the basis of this segmentation, we were able to distinguish undifferentiated stem cells from differentiated stem cells [19].

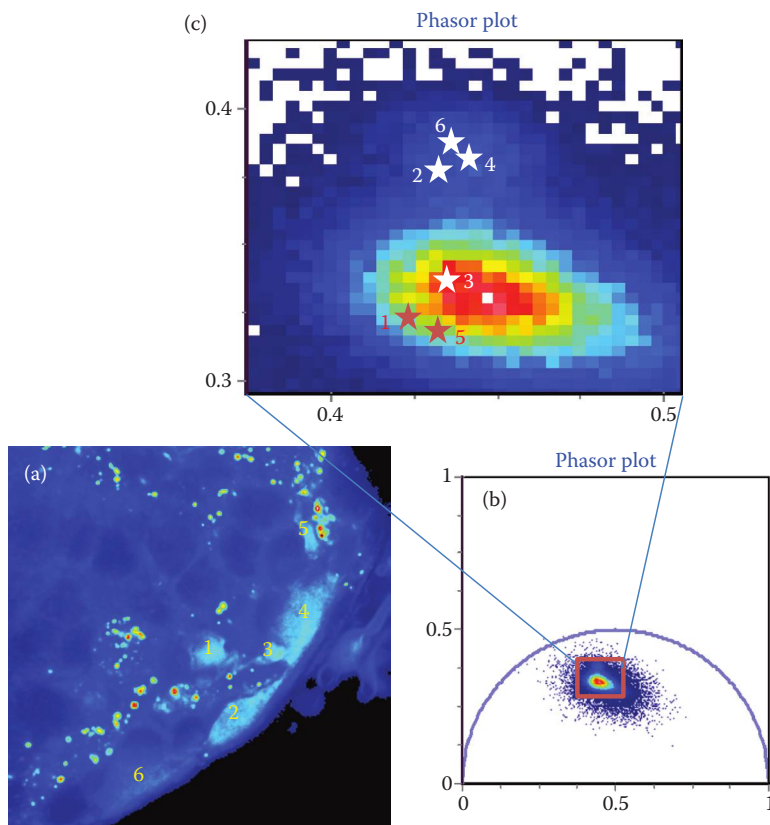


**Figure 10.12** Cell phasors. (a) Pixels in cells labeled 1 to 6 were selected for the calculation of the average value of the phasor in the cell region. (b) The phasor plot shows a superposition of many pixels. (c) Each cell has a different average phasor. Larger cells (2, 4, and 6) are the stem cells expressing the GFP-Oct4 gene. Cells 1, 3, and 5 are smaller cells.

## 10.9 CONCLUSIONS

The linear property of the phasor transformation is a powerful feature that allows a series of simple tools to be used to explore the phasor space. First, the most important point in this chapter on phasor analysis is the description of the filtering tool (image smoothing) that greatly decreases the noise in the phasor spread. This decrease in spread, based on the vector addition law, allows better identification of pixels with similar decay and better identification of linear combination of species. As a consequence of this law, if only two species are present in a pixel, all phasors must be contained in a narrow region of the phasor plot along the line joining the phasors of the pure species. If more (than two) species are present, we can use phasor plots at different harmonic frequencies to better separate their contributions. Since phasors add in the compound phasor histogram of many images, we can select portions of the phasor histogram based on the intensity image histogram. This property allows separation of apparently superimposing constitutions to the phasor plot.

All data analyses shown in this work have been performed using the SimFCS program that is available at the Laboratory for Fluorescence Dynamics website (<http://www.lfd.uci.edu/>). A number of tutorials that explain the use of this software also are available at this website.



## ACKNOWLEDGMENTS

The authors would like to acknowledge Claus Seidel, Chiara Stringari, and Elizabeth Hinde for providing some of the FLIM data used in this work. This work is supported in part by NIH-P41 P41-RRO3155, NIH P50-GM076516, and U54 GM064346.

## REFERENCES

1. Colyer, R., O. Siegmund, A. Tremsin, J. Vallerga, S. Weiss, and X. Michalet. 2009. Phasor-based single-molecule fluorescence lifetime imaging using a wide-field photon-counting detector. In *Single Molecule Spectroscopy and Imaging II*, edited by Jörg Enderlein, Zygmunt K. Gryczynski, Rainer Erdmann. *Proc. of SPIE* Vol. 7185, 71850T.
2. Grecco, H. E., P. Roda-Navarro, A. Girod, J. Hou, T. Frahm, D. C. Truxius, R. Pepperkok, A. Squire, and P. I. Bastiaens. 2010. In situ analysis of tyrosine phosphorylation networks by FLIM on cell arrays. *Nat Methods* 7:467–472.
3. James, N. G., J. A. Ross, M. Steff, and D. M. Jameson. 2011. Applications of phasor plots to in vitro protein studies. *Anal Biochem* 410:70–76.
4. Sanchez, S., L. Bakas, E. Gratton, and V. Herlax. 2011. Alpha hemolysin induces an increase of erythrocytes calcium: A FLIM 2-photon phasor analysis approach. *PLoS One* 6:e21127.
5. Digman, M. A., V. R. Caiolfa, M. Zamai, and E. Gratton. 2008. The phasor approach to fluorescence lifetime imaging analysis. *Biophys J* 94:L14–L16.
6. Chen, Y. C., and R. M. Clegg. 2009. Fluorescence lifetime-resolved imaging. *Photosynth Res* 102:143–155.
7. Matsubara, S., Y. C. Chen, R. Caliandro, Govindjee, and R. M. Clegg. 2011. Photosystem II fluorescence lifetime imaging in avocado leaves: Contributions of the lutein-epoxide and violaxanthin cycles to fluorescence quenching. *J Photochem Photobiol* 104:271–284.
8. Spring, B. Q., and R. M. Clegg. 2009. Image analysis for denoising full-field frequency-domain fluorescence lifetime images. *J Microsc* 235:221–237.
9. Behne, M. J., S. Sanchez, N. P. Barry, N. Kirschner, W. Meyer, T. M. Mauro, I. Moll, and E. Gratton. 2011. Major translocation of calcium upon epidermal barrier insult: Imaging and quantification via FLIM/Fourier vector analysis. *Arch Dermatol Res* 303:103–115.
10. Jameson, D. M., E. Gratton, and R. Hall. 1984. The measurement and analysis of heterogeneous emissions by multifrequency phase and modulation fluorometry. *App Spec Rev* 20:55–106.
11. Redford, G. I., and R. M. Clegg. 2005. Polar plot representation for frequency-domain analysis of fluorescence lifetimes. *J Fluoresc* 15:805–815.
12. Clayton, A. H., Q. S. Hanley, and P. J. Verveer. 2004. Graphical representation and multicomponent analysis of single-frequency fluorescence lifetime imaging microscopy data. *J Microsc* 213:1–5.
13. Gratton, E., S. Breusegem, J. Sutin, Q. Ruan, and N. Barry. 2003. Fluorescence lifetime imaging for the two-photon microscope: Time-domain and frequency-domain methods. *J Biomed Opt* 8:381–390.
14. Becker, W., A. Bergmann, M. A. Hink, K. König, K. Benndorf, and C. Biskup. 2004. Fluorescence lifetime imaging by time-correlated single-photon counting. *Microsc Res Tech* 63:58–66.
15. Lakowicz, J. R., G. Laczko, H. Cherek, E. Gratton, and M. Limkeman. 1984. Analysis of fluorescence decay kinetics from variable-frequency phase shift and modulation data. *Biophys J* 46:463–477.
16. Hodgson, L., O. Pertz, and K. M. Hahn. 2008. Design and optimization of genetically encoded fluorescent biosensors: GTPase biosensors. *Methods Cell Biol* 85:63–81.
17. Hodgson, L., F. Shen, and K. Hahn. 2010. Biosensors for characterizing the dynamics of rho family GTPases in living cells. *Curr Protoc Cell Biol* Chapter 14 (Unit 14. 11):1–26.
18. Celli, A., S. Sanchez, M. Behne, T. Hazlett, E. Gratton, and T. Mauro. 2010. The epidermal Ca(2+) gradient: Measurement using the phasor representation of fluorescent lifetime imaging. *Biophys J* 98:911–921.
19. Stringari, C., A. Cinquin, O. Cinquin, M. A. Digman, P. J. Donovan, and E. Gratton. 2011. Phasor approach to fluorescence lifetime microscopy distinguishes different metabolic states of germ cells in a live tissue. *Proc Natl Acad Sci USA* 108:13582–13587.